Robustness of Griffiths effects in homeostatic connectome models

Géza Ódor
Research Institute for Technical Physics and Materials Science, Centre for Energy Research of the Hungarian Academy of Sciences, P.O. Box 49, H-1525 Budapest, Hungary

(Received 22 October 2018; published 10 January 2019)

I provide numerical evidence for the robustness of the Griffiths phase (GP) reported previously in dynamical threshold model simulations on a large human brain network with $N = 836\,733$ connected nodes. The model, with equalized network sensitivity, is extended in two ways: introduction of refractory states or by randomized time-dependent thresholds. The nonuniversal power-law dynamics in an extended control parameter region survives these modifications for a short refractory state and weak disorder. In case of temporal disorder the GP shrinks and for stronger heterogeneity disappears, leaving behind a mean-field type of critical transition. Activity avalanche size distributions below the critical point decay faster than in the original model, but the addition of inhibitory interactions sets it back to the range of experimental values.

DOI: 10.1103/PhysRevE.99.012113

I. INTRODUCTION

Recent experimental evidence suggests [1,2] that our brain operates near criticality, where spatial and temporal correlations diverge [3], a dynamics that enhances the brain information-processing capabilities, increasing sensitivity and optimizing the dynamic range [4]. It might be the case that the brain tunes itself near criticality via self-organization (SOC) [5], or alternatively, could benefit from the same properties if sufficient heterogenities [6] (that is disorder) are present to induce an extended semicritical region, known as Griffiths phase (GP) [7]. Alternatively, it has recently been proposed that living systems may also self-tune to criticality as the consequence of evolution and adaptation [8]. The theory of phase transitions of statistical physics applied for these biological models can provide a clue to better understanding [9].

While SOC models [10] are usually *homogeneous*, real systems are highly *inhomogeneous* and one must consider if the heterogeneity is weak enough to apply "clean models" for the description of experiments. Strong disorder can lead to so-called rare-region (RR) effects [11] that smear the phase transitions [12,13]. RRs are very slowly relaxing domains, remaining in the opposite phase than the whole system for a long time, causing slow evolution of the order parameter. In the entire GP, which is an extended control parameter region around the critical point, fluctuations diverge and autocorrelations exhibit fat tailed, power-law (PL) behavior, causing burstyness [14]. Therefore, here one can observe dynamical critical behavior without the need of fine tuning. This was proposed to be the reason for the working memory in the brain [15] and considered to be a possible explanation for the observed criticality in neuroscience [16].

The seminal experiments by Beggs and Plenz [1] reported neuronal avalanches with size (s) dependence, defined as either the number of electrodes with suprathreshold activity or the sum of the potentials, according to a power law, $p(s) \propto s^{-1.5}$. For the duration distribution of such events $P(t) \propto t^{-2}$ PL tails were observed. These exponents are in agreement with the mean-field (MF) exponents of the directed percolation (DP) criticality: $\tau = 3/2$, $\tau_t = 2$, as well as with many other universality classes sharing the same MF avalanche exponents (see Refs. [17,18]). Mean-field exponents are expected to occur if the fluctuation effects are weak, when the system dimensionality is above the upper critical dimension D_c. For DP $D_c = 4$, but recent graph dimension measurements of large human connectomes suggest lower values [19]. Other experimental setups have revealed somewhat different exponents [20–22], suggesting different universal behaviors. Furthermore, Palva *et al.* [23] have found that source-reconstructed M/EEG data exhibit robust power-law long-range time correlations as well as scale-invariant avalanches with a broad range of exponents: $1 < \tau < 1.6$ and $1.5 < \tau_t < 2.4$. An obvious explanation for this wide spread of critical exponents can be heterogenities, which in the GP cause nonuniversal dynamical exponents [7,11,24].

It has been conjectured that network heterogeneity can cause GPs if the topological (graph) dimension D, defined by $N_r \sim r^D$, where N_r is the number of (j) nodes within topological distance $r = d(i, j)$ from an arbitrary origin (i), is finite [25]. This hypothesis has been supported numerically for various spreading models on scale-free graphs [26–28]. In the case of modular topological structure RRs are enhanced and Griffiths effects have been reported in synthetic brain networks with finite D [29–31] as well as in scale-free networks [32,33]. However, extended simulations of activity avalanches on very large human connectomes, possessing broad link weight distributions, did not support critical-like phase transition [34]. It turned out that in those graphs the weight heterogenities are too strong to allow the occurrence of RRs. This means that only the strongly connected hubs play a role in the activation and deactivation processes and weak nodes just follow them. This seems to be rather unrealistic and uneconomic in a brain of billions of neurons, thus some kind of input sensitivity equilibration was assumed via variable, node-dependent thresholds. This makes the system homeostatic and simulations proved the occurrence of criticality, as

well as Griffiths effects. Indeed, there is some evidence that neurons have a certain adaptation to their input excitation levels [35] and can be modeled by variable thresholds [36]. Recent theoretical studies have also suggested that homeostatic plasticity mechanisms may play a role in facilitating criticality [37–40]. Very recently comparison of modeling and experiments arrived at a similar conclusion: equalized network sensitivity improves the predicting power of a model at criticality in agreement with the FMRI correlations [41].

A two-state (active-inactive) stochastic threshold model with normalized input sensitivity [34], was investigated by simulations on a large, weighted human CC and the spatiotemporal behavior of activity avalanches was determined in the inactive phase. Numerical evidence has been found for a generic scale invariance in an extended control parameter space. Since this model may look to be too simplistic, especially for neuroscientists, now I extend it and perform numerical investigations of its dynamical behavior. The extensions are done in two directions. The addition of refractory states to the binary active-inactive model and the possibility of time-dependent thresholds. The refractory states happen for one time step following the active state of a node, thus an activated neighbor cannot activate back immediately, altering the spreading process. This is a common feature of brain models [42].

Time dependency of the network, which can be the consequence of some external fields, chemicals, or some cellular material distributed by the blood flow has been simulated by altering the thresholds randomly, in a synchronous way for all nodes. Such temporal disorder has been shown to lead to temporal Griffiths phases, resulting in algebraic size dependency (space-time flipped) [43,44] and enormous density fluctuations, characterized by an infinitely broad probability distribution at criticality. The combination of uncorrelated spatial and temporal disorder is irrelevant for the universal critical behavior [18], but correlated, diffusive spatiotemporal disorder has been found to be a relevant perturbation [45,46]. In this case I investigate the effect of long-range correlated spatiotemporal heterogeneity in the form of the addition of a time-dependent global sensitivity threshold to the quenched spatial disorder of the network.

II. MODELS AND METHODS

This study uses data from the open connectome project (OCP) [47], obtained by diffusion tensor imaging (DTI) [48] showing *structural brain connectivity* of the white matter. Other research on the structural networks have been much smaller sized. For example, the network obtained by Sporns and collaborators, using diffusion imaging techniques [49,50], consists of a highly coarse-grained mapping of anatomical connections in the human brain, comprising $N = 998$ brain areas and the fiber tract densities between them. The graph used here comprises $N = 848\,848$ nodes, allowing one to run extensive dynamical simulations on present day CPU and GPU clusters, still large enough to draw conclusions on the scaling behavior without the effects of finite sizes. Smaller systems near a critical phase transition point, where correlations diverge, suffer from finite-size corrections, which can hide true scaling region and RR effects.

These DTI connectomes of the human brain possess 1 mm^3 resolution, using a combination of diffusion weighted, functional, and structural magnetic resonance imaging scans. These graphs are symmetric, weighted networks, where the weights measure the number of fiber tracts between nodes. The large graph "KKI-18" used here is generated by the MIGRAINE method, described in Ref. [51]. These OCP graphs exhibit hierarchical levels by construction from the Desikan cerebral regions with (at least) two quite different scales. As it was discussed in Ref. [34] such coarse-grained CCs suffer possible sources of errors, like unknown noise in the data generation; underestimation of long connections; radial accuracy, influencing endpoints of the tracts and hierarchical levels of the cortical organization; or transverse accuracy, determining which cortical area is connected to another. Still, important modifications, such as inhibitory links, directedness, or random loss of connections up to 20%, confirmed the robustness of Griffiths effects, suggesting that fine network details may not play an important role. It is also important that the PL tail in the weight distribution is similar to what was obtained by a synaptic learning algorithm in an artificial neural network [52].

The investigated graph exhibits a single giant component of size $N = 836\,733$ nodes (out of $N = 848\,848$), 41 523 931 undirected edges and several small subcomponents, ignored here. In Ref. [19] we found that contrary to the small-world network coefficients OCP graphs exhibit topological dimension slightly above $D = 3$ [19] and certain amount of universality, supporting the selection of KKI-18 as a representative of the large human CCs available. This dimensionality suggests weak long-range connections, in addition to the $D = 3$-dimensional embedding ones and warrants to see heterogeneity effects in dynamical models defined on them. Further details are discussed in Refs. [19,34].

In my previous study [34] a two-state ($x_i = 0$ or 1) spreading model was used to describe the propagation, branching, and annihilation of activity on this network. This model is similar to those of Refs. [3,53], a discrete time stochastic cellular automata (SCA). The dynamical process, mimicking neuronal avalanches, is started by activating a randomly selected node. At each network update every (i) node is visited and tested if the sum of incoming weights ($w_{i,j}$) of active neighbors reaches a given threshold value

$$\sum_j x_j w_{i,j} > K. \tag{1}$$

If this condition is met a node activation is attempted with probability λ. Alternatively, an active node is deactivated with probability ν. New states of the nodes are overwritten only after a full network update; i.e., a synchronous update is performed at discrete time steps. The updating process continues as long as there are active sites or up to a maximum time limit $t = 10^6$ Monte Carlo sweeps (MCs). In case the system has fallen into inactivity, the actual time step is stored to calculate the survival probability $p(t)$ of runs. The average activity: $\rho(t) = 1/N \sum_{i=1}^{N} x_i$ and the number of activated nodes during the avalanche $s = \sum_{i=1}^{N} \sum_{t=1}^{T} x_i$ of duration is calculated at the end of the simulations. This SCA type of synchronous updating is not expected to affect the dynamical

scaling behavior [31] and provides a possibility for parallel algorithms. In fact, the code was implemented on GPUs, with 12× speedup with respect to good CPU cores [54]. Measurements on 10^6 to 10^7 independent runs, started from randomly selected, active initial sites, were averaged over for each control parameter value investigated.

In Ref. [34] I showed that this model running on the KKI-18 graph does not exhibit criticality, but due to the large weight differences and graph dimensionality hubs cause a catastrophic, discontinuous like transition. To keep the local sustained activity requirement for the brain [53] and avoid nodes that practically do not affect anything, I modified the model with variable thresholds of equalized sensitivity, by normalizing the incoming weights as $w'_{i,j} = w_{i,j} / \sum_{j \in \text{neighb.of } i} w_{i,j}$.

Now I extend this model with the addition of a refractory state, which occurs with nodes between an activation and deactivation event for one time step. This prevents activated neighbors from immediate reactivation of the source and one can expect to find propagating fronts, resembling dynamical percolation [18].

Another modification is the possibility for allowing a stochastic time dependence in the threshold value, by lowering K to $K - \Delta K$, with probability $1/2$ at each time MC step for all nodes. I tested here $\Delta K = 0.01, 0.02, 0.04, 0.05$ disorder strengths.

By varying the control parameters, K, λ, and ν, one can find a critical transition between an active and an absorbing steady state. At a critical point the survival probability of the activity avalanches (measured by the total number of active sites) is expected to scale asymptotically as

$$p(t) \propto t^{-\delta}, \tag{2}$$

where δ is the survival probability exponent [55]. This is related to the avalanche duration scaling $P(t) \propto t^{-\tau_t}$, via the relation [17]

$$\tau_t = 1 + \delta. \tag{3}$$

In the case of single active node initial conditions the number of active sites (measured by the total number of active sites during the spreading experiment) initially grows as

$$N(t) \propto t^{\eta}, \tag{4}$$

with the exponent η, which can be related to the avalanche size distribution

$$p(s) \propto s^{-\tau}, \tag{5}$$

via the scaling relation

$$\tau = (1 + \eta + 2\delta)/(1 + \eta + \delta), \tag{6}$$

This was derived in Ref. [17], assuming a bell-shaped distribution $p(s, t)$, which is the conditional probability of an avalanche having size s, given it dies at time t.

III. DYNAMICAL SIMULATION RESULTS

In Ref. [34] I compared results obtained on directed, randomly diluted edge variants of the KKI-18 network with those of the undirected graph and showed robustness of the GP for those changes. For simplicity I consider here the original KKI-18 network, which can be obtained from the graph, generated by the MIGRANE algorithm, after removing components, which do not belong to the largest connected one. The control parameter space was restricted by fixing $\lambda \simeq 1$, which mimics an efficient brain model and $\nu = 1$ or $\nu = 0.95$, corresponding to weak stochasticity in the deactivation transition. To see critical phase transition this requires a threshold value $K \simeq 0.2$. The time-dependent simulations were performed by selecting active initial sites randomly and by averaging over 10^7 realizations up to $t_{\max} = 3 \times 10^5$ Monte Carlo sweeps (MCs). Throughout the paper, time is measured in MCs.

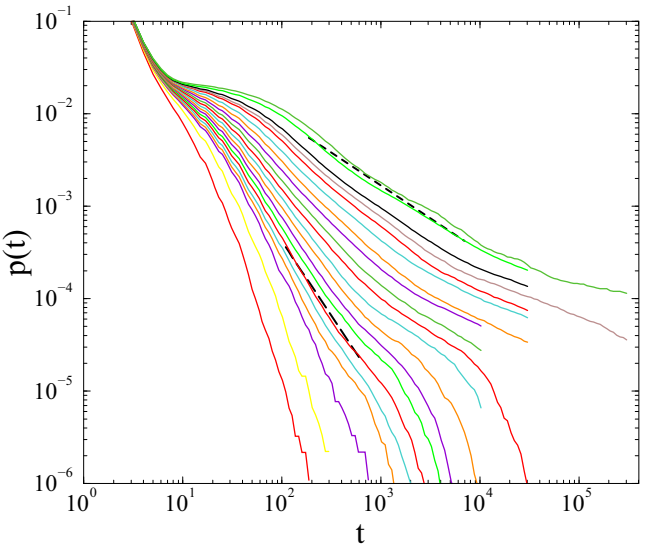

FIG. 1. Survival probability of the activity avalanches in case of refractory states. Parameters: $K = 0.2$, $\nu = 1$, and different $\lambda = 0.75, 0.8, 0.83, 0.84, 0.85, 0.86, 0.87, 0.88, 0.89, 0.9, 0.91, 0.92, 0.93, 0.94, 0.95, 0.96, 0.97, 0.98, 0.985$ (bottom to top curves). The dashed lines show PL fits for the tails of the curve $\lambda = 0.86$ as $\sim t^{-1.6(2)}$ and for the curve $\lambda = 0.98$ as $\sim t^{-0.70(4)}$.

A. Refractory state variable threshold model

Spreading simulations were run at $K = 0.2$ for different λ values. Figure 1 suggests a phase transition at $\lambda \simeq 0.985(4)$, above which $p(t)$ curves evolve to finite constant values. It is very hard to locate the transition clearly, since the evolution slows down and log-periodic oscillations also add, as the consequence of the modular network. Below the transition point we can find $p(t)$ decay curves with truncated PL tails, characterized by the exponents $0.7 < \delta < 1.6$, as we vary λ between $\simeq 0.84$ and 0.98. However, modulation of these PLs due to the modular network topology is also clearly visible. The lower-bound of the scaling region is rather uncertain and estimated by the λ value, where $p(t)$ and $\rho(t)$ seems to decay faster than a PL all for all times. Using the scaling relation Eq. (3) this means $1.7 < \tau_t < 2.6$, falling in the range of brain experiments: $1.5 < \tau_t < 2.4$ [23].

One can obtain even clearer PL tails for the density of active sizes $\rho(t)$ with smaller modulations (see the Fig. 2). The GP seems to stretch from $\lambda = 0.88$ with a linear

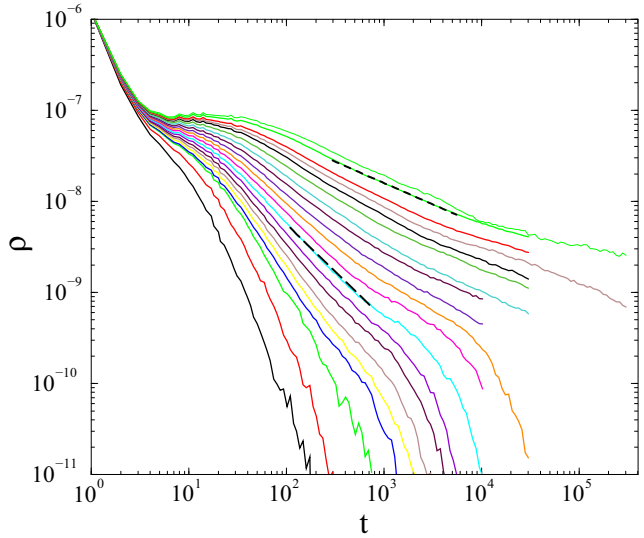

FIG. 2. Activity density decay in case of refractory states. Parameters: $K = 0.2$, $\nu = 1$, and different $\lambda = 0.75$, 0.8, 0.83, 0.84, 0.85, 0.86, 0.87, 0.88, 0.89, 0.9, 0.91, 0.92, 0.93, 0.94, 0.95, 0.96, 0.97, 0.98, 0.985 (bottom to top curves). The dashed lines show PL fits for the tails of the curve $\lambda = 0.86$ as $\sim 1/t$ and for the curve $\lambda = 0.98$ as $\sim t^{-0.47(1)}$.

deity decay to $\lambda = 0.98$, characterized by a PL fit for the tail $t^{-0.47(1)}$.

Finally, the avalanche size distributions (Fig. 3), exhibit clear PL tails, with continuously changing exponents in the range $1.4 < \tau < 1.91$, again in agreement with the brain experiments $1 < \tau < 1.6$ [23]. The results for the exponent τ can be crosschecked using the relation Eq. (6). For $\lambda = 0.98$ one obtains $\tau = 1.34(15)$, close to, but a little below, the direct measurements of avalanches: $\tau = 1.50(5)$.

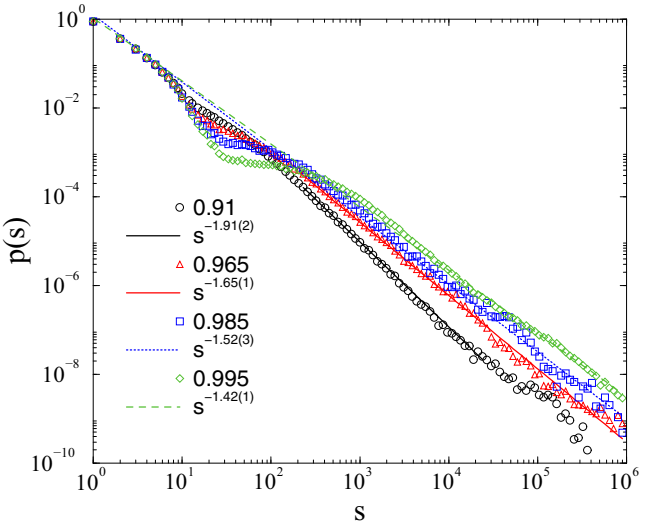

FIG. 3. Avalanche size distribution in the relative threshold model with refractory states, for $K = 0.2$, $\nu = 1$, and $\lambda = 0.91, 0.965, 0.985, 0.995$ (bottom to top symbols). Lines: PL fits for $10^2 < s < 10^5$, for these curves as shown by the legends.

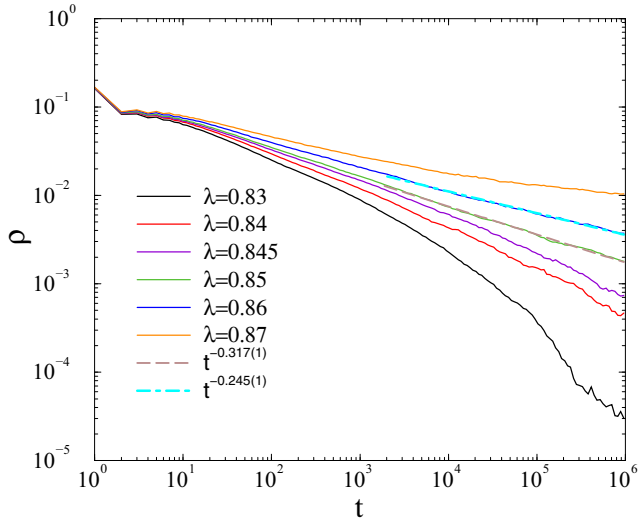

FIG. 4. Average density of activity in the equalized threshold model with time-dependent thresholds started from single active sites. Parameters: $K = 0.25$, $\Delta K = 0.02$, $\nu = 0.95$ and different $\lambda = 0.83, 0.84, 0.845, 0.85, 0.86, 0.87$ (bottom to top curve). Dashed line shows a PL fit $t^{-0.317(1)}$ for the tail of the $\lambda = 0.85$, while dot-dashed line shows PL fit $t^{-0.245(1)}$ for the $\lambda = 0.86$ curve. These exponents are away from the values of the three- or four-dimensional DP criticality, supporting a GP here.

B. Time-dependent thresholds

In the time-dependent variable threshold model, I fixed $\nu = 0.95$, $K = 0.25$ and performed spreading simulations using GPU-s, up to $t_{\max} = 10^6$ MCs. Before the application of the time-dependent thresholds the GPU accelerated algorithm was tested by the reproduction and extension of the results of [34] up to 10^7 MCs, up to two orders of higher values (see Sect. III C and [54]). Precise estimates for the critical point have been achieved for the model with inhibitory links (see Sect. III C).

In the case of the undirected graph, for $\nu = 0.95$, $K = 0.25$, I estimated a GP in the region $0.85 \leqslant \lambda \leqslant 0.95$ [34]. Now I investigate what happens if a weak temporal disorder is added. Binary distributed variable thresholds have been applied, first with $\Delta = 0.02$ as shown on Fig. 4.

The average density decays in a PL manner for $\lambda = 0.85$ and $\lambda = 0.86$ with slopes $\alpha = 0.317(1)$, $\alpha = 0.245(1)$, respectively. The $\lambda = 0.84$ curve seems to be subcritical, while the $\lambda = 0.87$ one is supercritical. Lowering the threshold occasionally results in supercritical control for $\lambda > 0.86$, which in the time-independent case was inside the GP. But part of the PL region seems to survive this perturbation.

The same conclusion can be drawn by considering the survival probabilities on Fig. 5, and we can see a narrower GP as before. It is important to note that these exponents are away from the values of the three- or four-dimensional DP criticality and those of Fig. 4, meaning the lack of rapidity reversal symmetry (see Ref. [18]).

In contrast, for stronger disorder, $\Delta = 0.04$, one can see a critical transition without the signs of any GP region. At the critical point $\lambda_c \simeq 0.78(1)$ one can fit decay $p(t) \propto t^{-0.9(1)}$ close to the MF value of DP (see Fig. 6). The same is true

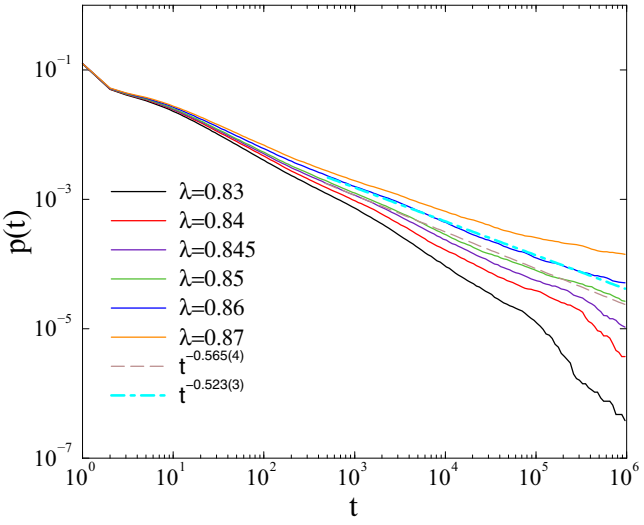

FIG. 5. Avalanche activity survival probability in the equalized threshold model with time-dependent thresholds, started from single active sites. Parameters: $K = 0.25$, $\Delta K = 0.02$, $\nu = 0.95$, and different $\lambda = 0.83, 0.84, 0.845, 0.85, 0.86, 0.87$ (bottom to top curve). Dashed line shows a PL fit $t^{-0.565(4)}$ for the tail of the $\lambda = 0.85$, while dot-dashed line shows a PL fit $t^{-0.523(3)}$ for the tail of the $\lambda = 0.86$ curve. These exponents are away from the values of the three- or four-dimensional DP criticality, supporting a GP here.

for the average density of activity. This suggests that this temporally applied "disorder" is strong enough to move all previous curves lying in the GP into the active phase, while the previously subcritical ones remain in the inactive.

The avalanche size distributions for $\Delta = 0.02$ also exhibit nonuniversal PLs in the GP, as shown in Fig. 7, with somewhat higher slope values: $p(s) \propto s^{-2.0(3)}$. For clarity I plotted

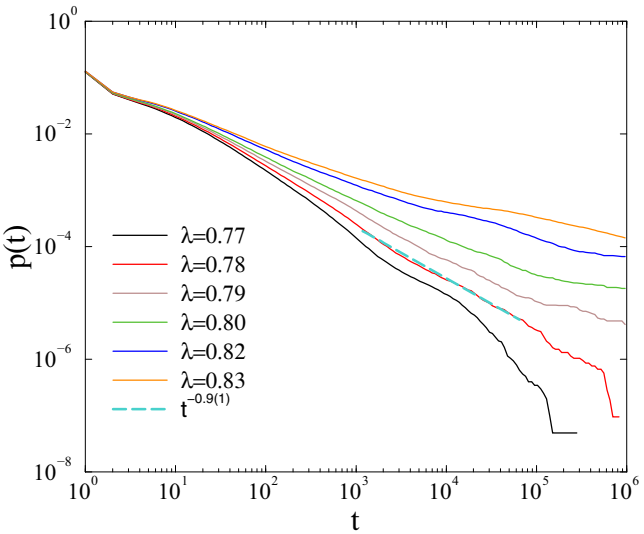

FIG. 6. Avalanche activity survival probability in the equalized threshold model with time-dependent thresholds, started from single active sites. Parameters: $K = 0.25$, $\Delta K = 0.04$, $\nu = 0.95$, and different $\lambda = 0.77, 0.78, 0.79, 0.80, 0.87$ (bottom to top curve). Dashed line shows PL fit $t^{-0.9(1)}$ for the tail of the $\lambda = 0.78$ curve.

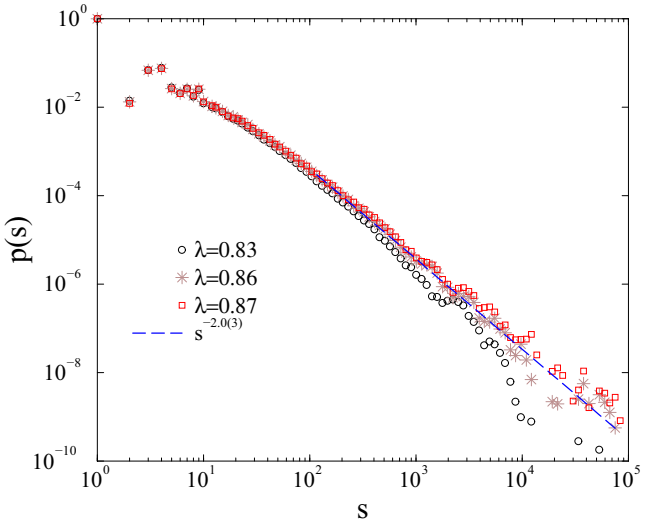

FIG. 7. Avalanche size distribution in the relative threshold model with time-dependent K-s. Parameters: $K = 0.25$, $\Delta K = 0.02$ $\nu = 0.95$, and $\lambda = 0.83, 0.86, 0.87$ (bottom to top symbols). Dashed line: PL fit for $10 < t < 1000$ of the $\lambda = 0.86$ (middle) case.

results for just three λ's, but the others fit well to them. This result for the exponent τ can be compared with the value we get via the scaling relation Eq. (6). For $\lambda = 0.86$ we can obtain $\tau = 1.31(15)$, away from the direct measurement. The reason behind it must be an asymmetric shaped $p(s, t)$ distribution, which has already been showed in Ref. [34]. Without this assumption inconsistent results were obtained in Ref. [56].

C. Time-dependent thresholds with inhibition

In real brain inhibitory neurons, suppressing communications of connections exist. I did not simulate such nodes explicitly but considered negative connections by fast inhibitory interneurons. To model this in Ref. [34] I changed 30% of the link weights as $w'_{i,j} = w_{i,j}$ randomly. This produces further heterogeneity, thus stronger RR effects. Figure 8 shows the survival probabilities, for $K = 0.1$ and $\nu = 0.95$. In this work I show the extension of the results presented in Ref. [34] by two orders of magnitude in time (from $t_{\max} = 10^5$ to $t_{\max} = 10^7$) using a GPU code, with the primary aim to confirm the parallel program, and with the secondary aim to provide more precise results at the critical point and for the GP.

The critical point, above which $p(t)$ signals persistent activity, is around $\nu = 0.56(1)$, hard to locate clearly, since the evolution slows down and exhibit strong (oscillating) corrections. Here ultraslow, log scaling tail can be observed of the form $p(t) \propto \ln(t)^{-0.84(1)}$, as the left inset of Fig. 8 shows. This value is smaller than what was found in Ref. [34], for the original, positive weighted graph, $\tilde{\delta} = 3.5(3)$, suggesting a lower effective topological dimension due to the inhibitions. For comparison, in the case of spatially quenched disordered models belonging to the same universality class in one dimension, $\tilde{\delta} = 0.38187$ [57], while in two-dimensions, $\tilde{\delta} = 1.9(2)$ [58].

Below the transition point the survival exponent changes continuously in the range $0 < \delta < 0.5$ as a response for the variation of ν between 0.5 and 0.57 (right inset of Fig. 8). To

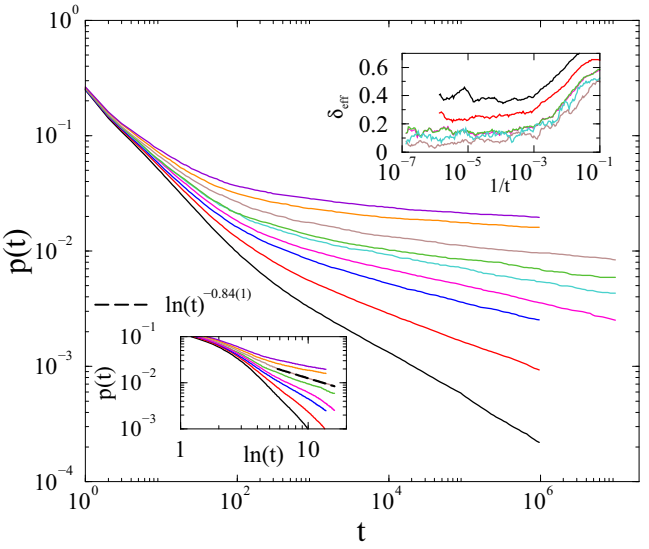

FIG. 8. Extension of the simulations for the variable threshold model with inhibitory links of Ref. [34]. Avalanche survival probability decay of the relative threshold model with 30% inhibitory links at $K = 0.1$, for $\nu = 0.95$ and $\lambda = 0.5$, 0.51, 0.52, 0.53, 0.54, 0.55 0.555, 0.56, 0.57 (bottom to top curves). Lower left inset: the same data as the function of $\ln(t)$. Dashed line: logarithmic scaling fit for the tail of $\lambda = 0.555$ curve. Upper right inset: local slopes of the same curves in opposite order showing saturation of the nonuniversal exponents in the GP.

see corrections to scaling I determined the local slopes of the dynamical exponents δ as the discretized, logarithmic derivative of Eq. (2). The effective exponent of δ is measured as

$$\delta_{\rm eff}(t) = -\frac{\ln p(t) - \ln p(t')}{\ln(t) - \ln(t')}, \tag{7}$$

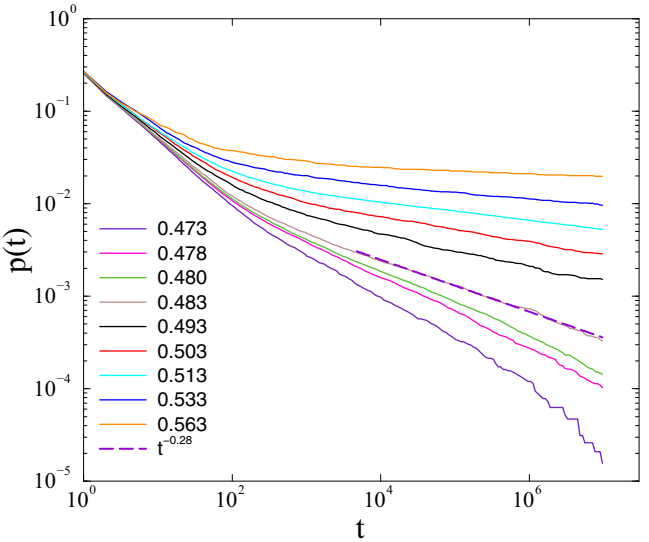

FIG. 9. Avalanche survival probability decay of the relative threshold model with 30% inhibitory links at $K = 0.1$ and $\Delta K = 0.01$, for $\nu = 0.95$ and $\lambda = 0.473$, 0.478, 0.48, 0.483, 0.493, 0.503, 0.513, 0.533, 0.563 (bottom to top curves). The dashed line shows a PL fit $t^{-0.28(1)}$ for the tail of the $\lambda = 0.483$ curve.

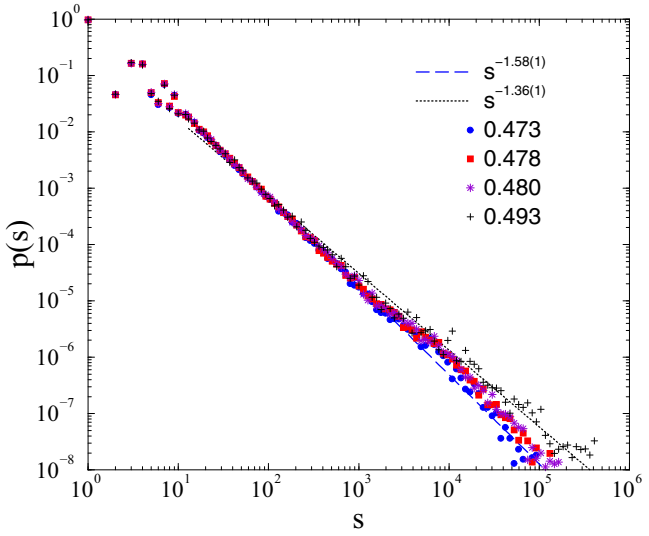

FIG. 10. Avalanche size distribution of the time-dependent relative threshold model with 30% inhibitory links at $K = 0.1$, $\Delta K = 0.01$, $\nu = 0.95$, and $\lambda = 0.473, 0.478, 0.480, 0.493$ (bottom to top symbols). Dashed lines: PL fits for the tails of the $\lambda = 0.473$ and $\lambda = 0.493$ curves (bottom to top).

using $t - t' = 8$. A remarkable stabilization of $\delta_{\rm eff}$ can be observed for $10^4 < t < 10^7$ in the GP.

As in Sec. III B, I applied time-dependent thresholds by lowering $K = 0.1$ to $K = 0.09$ at random time steps with probability 0.5. In this case, the GP shrunk to the region $0.483 < \lambda < 0.513$ approximately (see Fig. 9). Thus, the critical point moved down to $\lambda \simeq 0.51(1)$ with respect to the time-independent model. Near the critical point the avalanche size distributions exhibit roughly $p(s) \propto t^{-1.5}$ PL tails in agreement with experiments as shown on Fig. 10. Furthermore, the exponents decrease slightly by increasing λ.

Similarly to the noninhibitory case, for larger temporal disorder, i.e., for $\Delta K = 0.05$ one cannot see clear PLs, or maybe just in a narrow region, hindered by strong periodic modulations. Location of the phase transition point in this case is hard, but one can estimate it to be $\lambda \simeq 0.40(1)$. The avalanche size distributions exhibit $p(s) \propto s^{-1.4}$ PL tails here, but extended GP cannot be observed now.

IV. DISCUSSION AND CONCLUSIONS

I have extended the dynamical scaling study of the activity behavior of the connectome model started in Ref. [34] with the addition of refractory states and time-dependent threshold values. High-precision simulations showed the survival of GP in both cases, albeit in case of temporal disorder the GP shrinks. By lowering or increasing the threshold occasionally, RRs of the original GP feel super- or subcritical "quenches." Thus, their evolutions do not follow the slow dynamics with large characteristic times. In the case of the addition of refractory states, the GP seems to be even wider as in the two-state model. The avalanche size distributions exhibit fat tails with control-parameter-dependent PL exponents near the MF value, but the τ exponent does not satisfy the scaling law Eq. (6) connecting it to δ and η in general, suggesting asymmetric $p(s|t)$ distributions like in Ref. [34].

In summary, while in the case of quasistatic, nonequalized threshold models fat tail distributed weights exclude rare-region effects (thus a GP), in equalized ones, simulations provide numerical evidence for robust occurrence of Griffiths effects for susceptible-excited-susceptible type of models [34], for susceptible-excited-refractory-susceptible models, even in the case of weak temporal noise. Inhibitory weights do not alter this scenario qualitatively but provide homeostatic states in which the scaling behavior is quantitatively more similar to the brain experiments.

In particular, for the susceptible-excited-refractory-susceptible model the duration exponents in the GP are $1.7 < \tau_t < 2.6$, while the avalanche size exponents are in the range $1.4 < \tau < 1.91$. For the weakly time-dependent ($\Delta = 0.02$) susceptible-excited-susceptible model, one can estimate $1.5 < \tau_t < 1.7$ and $2 < \tau < 2.28$. In the case of inhibition, the scaling exponents of the weakly time-dependent, susceptible-excited-susceptible model least squares fitting and Eq. (6) results in $1 < \tau_t < 1.5$, $1.1 < \tau < 1.6$. In general, for the durations a minimum value may emerge as $\tau_t = 1+\delta > 1$, as a consequence of a nonconventional critical point, at the top of the GP in case of logarithmic scaling. For the avalanche size distributions there is no such minimum value of $\tau = 2.2$ reported in a fuse model, which is defined on hierarchical modular networks [59]. Instead, the simulations on this connectome, or in the case of nonhierarchical modular networks [33] $\tau < 1$ can be observed only.

Simultaneous, interacting avalanches should not alter the global universal dynamical critical exponents in statistical physics, although one can speculate how to define an avalanche in this case. If one could measure the activity spreading causally, one could decide if activated nodes are distinguishable or not. In the former case one can apply a neutral theory and obtain scale-free dynamics even away from the edge of a phase transition [60]. In the latter case I believe one should not obtain different critical behavior, like in case of identical multicomponent reaction-diffusion systems in higher dimensions [18]. In a more realistic model, exhibiting memory of nodes in accumulating action potentials, interacting avalanches can influence their mutual spreading behavior, like for a pair-contact process [18] and initial condition-dependent scaling may also emerge.

It is important to stress that this study does not aim to exclude SOC-generating synaptic learning and plasticity mechanisms, leading to homeostatic states and closeness of a criticality in brain models. Instead of that I show how heterogeneities alter the dynamical behavior, causing critical-like PLs in an extended control parameter region even below the singular phase transition point and provide a possible explanation for the spread of exponents measured. Experimental justification of GP would require measuring the avalanche and autocorrelation exponents in high resolution and show how the scattered exponents depend on some control parameters (sensitivity, inhibition, etc.) of the brain. An interesting continuation of this work would be to test *partially* equalized input sensitivities, where first-order phase transition was shown [34], in agreement with brain experiments, showing abrupt transition between up and down states; see Ref. [61].

The codes and the graph used here are available on request from the author.

ACKNOWLEDGMENTS

I thank Vince Varga for developing the GPU code and appreciate the comments from M. Palva, M. Gastner, and R. Juhász. The simulations have been performed on the NIIF HPC Hungarian national supercomputer machines. Support from the Hungarian research fund OTKA (Grants No. K109577 and No. K128989) is acknowledged.

[1] J. Beggs and D. Plenz, Neuronal avalanches in neocortical circuits, J. Neurosci. **23**, 11167 (2003).
[2] D. R. Chialvo, Emergent complex neural dynamics, Nat. Phys. **6**, 744 (2010).
[3] A. Haimovici, E. Tagliazucchi, P. Balenzuela, and D. R. Chialvo, Brain Organization into Resting State Networks Emerges at Criticality on a Model of the Human Connectome, Phys. Rev. Lett. **110**, 178101 (2013).
[4] D. B. Larremore, W. L. Shew, and J. G. Restrepo, Predicting Criticality and Dynamic Range in Complex Networks: Effects of Topology, Phys. Rev. Lett. **106**, 058101 (2011).
[5] P. Bak, C. Tang, and K. Wiesenfeld, Self-organized criticality, Phys. Rev. A **38**, 364 (1988).
[6] B. B. Lake *et al.*, Neuronal subtypes and diversity revealed by single-nucleus RNA sequencing of the human brain, Science **352**, 1586 (2016).
[7] R. B. Griffiths, Nonanalytic Behavior Above the Critical Point in a Random Ising Ferromagnet, Phys. Rev. Lett. **23**, 17 (1969).
[8] J. Hidalgo *et al.*, Information-based fitness and the emergence of criticality in living systems, Proc. Natl. Acad. Sci. USA **111**, 10095 (2014).
[9] M. A. Mñoz, Colloquium: Criticality and dynamical scaling in living systems, Rev. Mod. Phys. **90**, 031001 (2018).
[10] G. Pruessner, *Self Organized Criticality* (Cambridge University Press, Cambridge, 2012).
[11] T. Vojta, Rare region effects at classical, quantum, and nonequilibrium phase transitions, J. Phys. A: Math. Gen. **39**, R143 (2006).
[12] P. M. Villa Martin, J. A. Bonachela, and M. A. Muñoz, Quenched disorder forbids discontinuous transitions in nonequilibrium low-dimensional systems, Phys. Rev. E **89**, 012145 (2014).
[13] P. M. Villa Martin, M. Moretti, and M. A. Muñoz, Rounding of abrupt phase transitions in brain networks, J. Stat. Mech. (2015) P01003.
[14] G. Ódor, Slow, bursty dynamics as a consequence of quenched network topologies, Phys. Rev. E **89**, 042102 (2014)
[15] S. Johnson, J. J. Torres, and J. Marro, Robust short-term memory without synaptic learning, PLoS ONE **8**, e50276 (2013)
[16] C. C. Hilgetag and M.-T. Hutt, Hierarchical modular brain connectivity is a stretch for criticality, Trends Cogn. Sci. **18**, 114 (2013).
[17] M. A. Muñoz, R. Dickman, A. Vespignani, and S. Zapperi, Avalanche and spreading exponents in systems with absorbing states, Phys. Rev. E **59**, 6175 (1999).

[18] G. Ódor, Universality classes in nonequilibrium lattice systems, Rev. Mod. Phys. **76**, 663 (2004).

[19] M. T. Gastner and G. Ódor, The topology of large open connectome networks for the human brain, Sci. Rep. **6**, 27249 (2016).

[20] N. Friedman, S. Ito, B. A. W. Brinkman, M. Shimono, R. E. DeVille, K. A. Dahmen, J. M. Beggs, and T. C. Butler, Universal Critical Dynamics in High Resolution Neuronal Avalanche Data, Phys. Rev. Lett. **108**, 208102 (2012).

[21] W. L. Shew, W. P. Clawson, J. Pobst, Y. Karimipanah, N. C. Wright, and R. Wessel, Adaptation to sensory input tunes visual cortex to criticality, Nat. Phys. **11**, 659 (2015).

[22] M. Yaghoubi *et al.*, Neuronal avalanche dynamics indicates different universality classes in neuronal cultures, Sci. Rep. **8**, 3417 (2018).

[23] J. M. Palva, A. Zhigalov, J. Hirvonen, O. Korhonen, K. Linkenkaer-Hansen, and S. Palva, Neuronal long-range temporal correlations and avalanche dynamics are correlated with behavioral scaling laws, Proc. Natl. Acad. Sci. USA **110**, 3585 (2013).

[24] Strictly speaking, we cannot prove GP in finite models without the possibility of showing size independence, as in the case of the available connectome graphs, but Griffiths effects.

[25] M. A. Muñoz, R. Juhász, C. Castellano, and G. Ódor, Griffiths Phases on Complex Networks, Phys. Rev. Lett. **105**, 128701 (2010).

[26] G. Ódor and R. Pastor-Satorras, Slow dynamics and rare-region effects in the contact process on weighted tree networks, Phys. Rev. E **86**, 026117 (2012).

[27] G. Ódor, Rare regions of the susceptible-infected-susceptible model on Barabáasi-Albert networks, Phys. Rev. E **87**, 042132 (2013).

[28] G. Ódor, Spectral analysis and slow spreading dynamics on complex networks, Phys. Rev. E **88**, 032109 (2013).

[29] P. Moretti and M. A. Muñoz, Griffiths phases and the stretching of criticality in brain networks, Nat. Commun. **4**, 2521 (2013).

[30] P. Villegas, P. Moretti, and M. A. Muñoz, Frustrated hierarchical synchronization and emergent complexity in the human connectome network, Sci. Rep. **4**, 5990 (2014)

[31] G. Ódor, R. Dickman, and G. Ódor, Griffiths phases and localization in hierarchical modular networks, Sci. Rep. **5**, 14451 (2015).

[32] W. Cota, S. C. Ferreira, and G. Ódor, Griffiths effects of the susceptible-infected-susceptible epidemic model on random power-law networks, Phys. Rev. E **93**, 032322 (2016).

[33] W. Cota, S. C. Ferreira, and G. Ódor, Griffiths phases in infinite-dimensional, non-hierarchical modular networks, Sci. Rep. **8**, 9144 (2018).

[34] G. Ódor, Critical dynamics on a large human open connectome network, Phys. Rev. E **94**, 062411 (2016).

[35] R. Azouz and C. M. Gray, Dynamic spike threshold reveals a mechanism for synaptic coincidence detection in cortical neurons in vivo, Proc. Natl. Acad. Sci. USA **97**, 8110 (2000).

[36] M.-T. Hütt, M. K. Jain, C. C. Hilgetag, and A. Lesne, Stochastic resonance in discrete excitable dynamics on graphs, Chaos Solitons Fractals **45**, 611 (2012).

[37] F. Droste, A.-L. Do, and T. Gross, Analytical investigation of self-organized criticality in neural networks, J. R. Soc. Interface **10**, 20120558 (2013).

[38] G. Deco, A. Ponce-Alvarez, P. Hagmann, G. L. Romani, D. Mantini, and M. Corbetta, How local excitation-inhibition ratio impacts the whole brain dynamics, J. Neurosci. **34**, 7886 (2014).

[39] P. J. Hellyer, B. Jachs, C. Clopath, and R. Leech, Local inhibitory plasticity tunes macroscopic brain dynamics and allows the emergence of functional brain networks, NeuroImage **124**, 85 (2015).

[40] P. J. Hellyer, C. Clopath, A. A. Kehagia, F. E. Turkheimer, and R. Leech, From homeostasis to behavior: Balanced activity in an exploration of embodied dynamic environmental-neural interaction, PLoS Comput. Biol. **13**, e1005721 (2017).

[41] R. P. Rocha, L. Koçillari, S. Suweis, M. Corbetta, and A. Maritan, Homeostatic plasticity and emergence of functional networks in a whole-brain model at criticality, Sci. Rep. **8**, 15682 (2018).

[42] E. R. Kandel, *Principles of Neural Science*, 5th ed. (The MCGraw-Hill Companies, New York, 2013).

[43] F. Vazquez, J. A. Bonachela, C. López, and M. A. Muñoz, Temporal Griffiths Phases, Phys. Rev. Lett. **106**, 235702 (2011).

[44] T. Vojta and J. A. Hoyos, Infinite-noise criticality: Nonequilibrium phase transitions in fluctuating environments, Europhys. Lett. **112**, 30002 (2015).

[45] R. Dickman, A contact process with mobile disorder, J. Stat. Mech. (2009) P08016.

[46] T. Vojta and R. Dickman, Spatiotemporal generalization of the Harris criterion and its application to diffusive disorder, Phys. Rev. E **93**, 032143 (2016).

[47] See https://neurodata.io.

[48] B. A. Landman *et al.*, Multi-parametric neuroimaging reproducibility: A 3-T resource study, NeuroImage **54**, 2854 (2011).

[49] P. Hagmann *et al.*, Mapping the Structural Core of Human Cerebral Cortex, PLoS Biol. **6**, e159 (2008).

[50] C. J. Honey *et al.*, Predicting human resting-state functional connectivity from structural connectivity, Proc. Natl. Acad. Sci. USA **106**, 2035 (2009).

[51] W. G. Roncal *et al.*, MIGRAINE: MRI graph reliability analysis and inference for connectomics, in *Proceedings of the IEEE Global Conference on Signal and Information Processing* (John Hopkins University, Maryland, USA, 2013), pp. 313–316.

[52] S. Scarpetta, I. Apicella, L. Minati, and A. de Candia, Hysteresis, neural avalanches, and critical behavior near a first-order transition of a spiking neural network, Phys. Rev. E **97**, 062305 (2018).

[53] M. Kaiser and C. C. Hilgetag, Optimal hierarchical modular topologies for producing limited sustained activation of neural networks, Front. Neuroinf. **4**, 8 (2010).

[54] G. Ódor and V. Varga, Simulation of whole brain models on large human connectomes, poster preseted in GTC2018 Conference San Jose, CA, 2018, https://www.nvidia.com/en-us/gtc/poster-gallery/hpc-and-supercomputing/.

[55] P. Grassberger and A. de la Torre, Reggeon field theory (Schlögl's first model) on a lattice: Monte Carlo calculations of critical behaviour, Ann. Phys. **122**, 373 (1979).

[56] A. Chessa, H. E. Stanley, A. Vespignani, and S. Zapperi, Universality in sandpiles, Phys. Rev. E **59**, R12 (1999).

[57] J. Hooyberghs, F. Iglói, and C. Vanderzande, Strong Disorder Fixed Point in Absorbing-State Phase Transitions, Phys. Rev. Lett. **90**, 100601 (2003).

[58] I. A. Kovács and F. Iglói, Infinite-disorder scaling of random quantum magnets in three and higher dimensions, Phys. Rev. B **83**, 174207 (2011).

[59] P. Moretti, B. Dietemann, and M. Zaiser, Avalanche precursors of failure in hierarchical fuse networks, Sci. Rep. **8**, 12090 (2018).

[60] M. Martinello, J. Hidalgo, A. Maritan, S. di Santo, D. Plenz, and M. A. Muñoz, Neutral Theory and Scale-Free Neural Dynamics, Phys. Rev. X **7**, 041071 (2017).

[61] D. A. McCormick, Neuronal Networks: Flip-Flops in the Brain, Curr. Biol. **15**, R294 (2005).